Available online at www.sciencedirect.com
ScienceDirect
Catalysis Today 123 (2007) 86–93
CATALYSIS TODAY
www.elsevier.com/locate/cattod

Oxidation entropies and enthalpies of ceria–zirconia solid solutions

Gong Zhou [a], Parag R. Shah [a], Taeyoon Kim [a], Paolo Fornasiero [b], Raymond J. Gorte [a,*]

[a] Department of Chemical and Biomolecular Engineering, University of Pennsylvania, Philadelphia, PA 19104, USA
[b] Chemistry Department, INSTM, Trieste RU and Centre of Excellence for Nanostructured Materials, University of Trieste, Via L. Giorgieri 1, I-34127 Trieste, Italy

Available online 19 January 2007

Abstract

The thermodynamic redox properties for a series of ceria–zirconia solid solutions have been measured by determining their oxidation isotherms between 873 and 1073 K. Isotherms were obtained using Coulometric titration and using O_2 titration of samples equilibrated in flowing mixtures of H_2 and H_2O. Samples having the following compositions were studied after calcinations at 973 and 1323 K: CeO_2, $Ce_{0.92}Zr_{0.08}O_2$, $Ce_{0.81}Zr_{0.19}O_2$, $Ce_{0.59}Zr_{0.41}O_2$, $Ce_{0.50}Zr_{0.50}O_2$, $Ce_{0.25}Zr_{0.75}O_2$, $Ce_{0.14}Zr_{0.86}O_2$, and ZrO_2. While the oxidation enthalpy for CeO_2 was between −750 and −800 kJ/mol O_2, the oxidation enthalpies for each of the solid solutions were between −500 and −550 kJ/mol O_2 and essentially independent of the extent of reduction. The shapes of the isotherms for the solid solutions were affected by the oxidation entropies, which depended strongly on the sample composition and the extent of reduction. With CeO_2, $Ce_{0.92}Zr_{0.08}O_2$, and $Ce_{0.14}Zr_{0.86}O_2$, the samples remained single-phase after calcination at 1323 K and the thermodynamic redox properties were unaffected. By contrast, $Ce_{0.59}Zr_{0.41}O_2$ formed two phases following calcination at 1323 K, $Ce_{0.78}Zr_{0.22}O_2$ (71 wt.%) and $Ce_{0.13}Zr_{0.87}O_2$ (29 wt.%); the isotherm changed to that which would be expected for a physical mixture of the two phases. A model is presented which views reduction of the solid solutions in terms of the local atomic structure, with the formation of ''pyrochlore-like'' clusters causing the increased reducibility of the solid solutions. Some of the changes in reducibility are associated with the number of sites from which oxygen can be removed in order to form pyrochlore-like clusters.

Keywords: Ceria–zirconia; Coulometric titration; Thermodynamic properties; Reduction enthalpy; Entropy

1. Introduction

Ceria–zirconia solid solutions are important for providing oxygen-storage capacitance (OSC) in automotive three-way catalysts [1–7]. The solid solutions are also finding new applications as supports for water–gas-shift catalysts [8–15] and as promoters in other reactions [16–20]. Ceria–zirconia solid solutions are typically used, rather than pure ceria, because the solid solutions are more easily reduced than pure ceria. The higher OSC of the solid solutions has sometimes been attributed to the mixtures having higher surface areas after thermal treatments [21], but it seems clear that other factors also play a role [6,21–25]. For example, thermodynamic calculations using literature data for pure ceria show that it should not be possible to substantially reduce ceria in gas-phase mixtures with H_2:H_2O or CO:CO_2 ratios less than 10 at temperatures less than 973 K [26–33]. Since automotive exhaust is always more oxidizing than this, i.e. there is always much more steam than H_2 in automotive exhausts, these calculations imply that ceria should not be able to provide oxygen storage.

Clearly, the materials used for OSC must differ significantly from the high-temperature forms of ceria that have been used to obtain the thermodynamic data that is in the literature. Furthermore, determination of thermodynamic properties, including oxidation enthalpies and entropies, would seem to be crucial for understanding how ceria-based catalysts function. Because there is relatively little data available on the thermodynamic properties of ceria–zirconia solid solutions [34], our laboratories have begun the measurement of these properties in order to understand how zirconia affects the oxidation and reduction of $CeO_{(2-x)}$ [35,36]. Our approach for obtaining thermodynamic parameters has been to measure equilibrium isotherms. For example, at any specific temperature, there is an O_2 fugacity, $P(O_2)$, that is in equilibrium with $CeO_{(2-x)}$ [26–33]. The range of $P(O_2)$ values that are of interest

* Corresponding author. Tel.: +1 215 898 4439; fax: +1 215 573 2093.
E-mail address: gzhou@seas.upenn.edu (G. Zhou).

0920-5861/$ – see front matter
doi:10.1016/j.cattod.2007.01.013

for equilibrium measurements is so low as to be experimentally inaccessible, making it necessary to establish $P(O_2)$ through equilibrium with H_2 oxidation, $H_2 + 1/2O_2 = H_2O$. Low values for $P(O_2)$ can then be achieved through gas-phase mixtures of H_2O and H_2, according to Eq. (1):

$$P(O_2)^{1/2} = K_{\text{equilib}}^{-1} \frac{P(H_2O)}{P(H_2)} \quad (1)$$

The equilibrium constant for oxidation of a metal oxide, such as $CeO_{(2-x)}$, is directly related to $P(O_2)$, since the activities of solid phases are one. Therefore, the measurement of $P(O_2)$ as a function of x provides the equilibrium constant and the Gibbs free energy, ΔG, for reaction at that value of x. Oxidation enthalpies, ΔH, can be determined by measuring isotherms at different temperatures, using Eq. (2):

$$\Delta H = \left. \frac{-R\,\delta \ln(P(O_2))}{\delta(1/T)} \right|_x \quad (2)$$

Previous work from our laboratories focused on ceria-rich materials, with most of the samples having more than 50% Ce [35]. While a few samples were examined after high-temperature calcination, this was avoided in past work for materials that undergo phase separation. In the present paper, we will first review the previous results from our laboratories, and then extend the data to include equilibrium properties for Zr-rich, solid solutions. Finally, we will report isotherm data on samples that underwent a phase change following high-temperature calcination. In all cases, the redox properties of the mixed oxides depended strongly on the composition of the phases that were present. The oxidation enthalpies for reduction of the solid solutions were significantly different from that of pure ceria but were essentially independent of Zr content. This result implies that oxygen binding is very localized, not dependent on long-range structure. By contrast, oxidation entropies changed dramatically with composition and extent of reduction, a result that can be rationalized based on the number of ways oxygen can be removed from localized clusters.

2. Experimental

2.1. Samples

Ceria–zirconia solid solutions were prepared using the citric acid method as described in a previous paper [37]. Stoichiometric amounts of $Ce(NO_3)_3$ and $ZrO(NO_3)_2{}^{\bullet}xH_2O$ were dissolved in distilled water and then mixed with aqueous citric acid (≥99.5%, Aldrich) to produce a solution with a citric-acid:metal-ion ratio of 1:2. The solutions were stirred vigorously at room temperature for 1 h and then the water was removed by evaporation. Finally, the resulting solids were heated in air at 723 K for 5 h to produce the solid solutions. Additional calcinations at 973 or 1323 K were used to check the phase stability of the $Ce_yZr_{1-y}O_2$ samples and to determine the effect of calcination temperature on the equilibrium properties. The samples that were studied are listed in Table 1, along with some of their properties.

Table 1
A list of materials used in this study

Sample	Calcination temperature[a] (K)	Crystallite size (Å)	Lattice constant (Å)
CZ 100/0	723	158	5.4171 (5.4124[b])
	973	–	–
	1173	1086	5.4149
CZ 92/8	973	135	5.3997 (5.3945[b])
	1323	669	5.3957
CZ 81/19	973	174	5.3693 (5.3648[b])
	1323	543	5.3662
CZ 59/41	973	181	5.3056 ((5.3054[b])
	1323	362	–
CZ 50/50	973	168	5.2852 (5.2811[b])
CZ 25/75	973	102	5.2018
	1323	–	–
CZ 14/86	973	84	5.1589
	1323	258	–

[a] The samples were calcined at 723 K for 5 h, 973 K for 48 h and at 1323 K for 4 h.
[b] The lattice parameters were calculated by Vegard's rule using the values from JCPDS file.

The phase compositions and structures of the samples were determined by X-ray diffraction (XRD), using a Cu Kα radiation source (λ = 1.5405 Å). Fig. 1, which shows representative XRD data for a range of ceria–zirconia solutions, indicates that all of the solid solutions appear to be cubic and single phase after calcination at 973 K. The lattice constants for each sample could be calculated using the location of the (2 2 0) diffraction peak. While ceria–zirconia solid solutions with intermediate compositions may form meta-stable tetragonal phases [37], it is difficult to distinguish this from a cubic phase using XRD alone, particularly with broad diffraction peaks. The relationship between the lattice constant and the Zr^{4+} concentration in ceria–zirconia solutions has been reported [37], so that the lattice parameters provided a check of the sample compositions. In each case, the calculated compositions

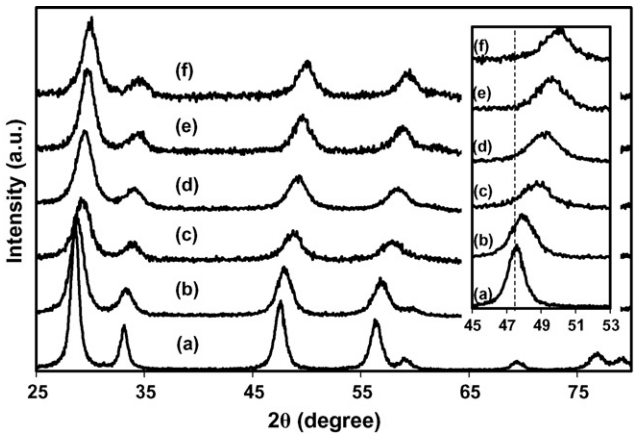

Fig. 1. XRD patterns for $Ce_yZr_{1-y}O_2$ samples following calcination at 973 K: (a) $y = 1$, (b) $y = 0.81$, (c) $y = 0.5$, (d) $y = 0.33$, (e) $y = 0.25$, and (f) $y = 0.14$. The inset shows an expanded view of (2 2 0) peak for each sample.

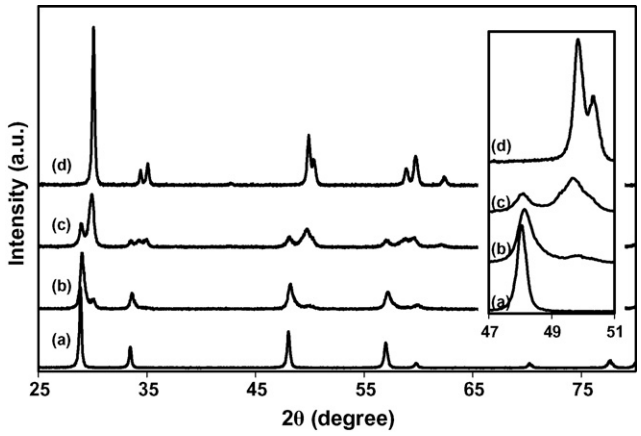

Fig. 2. XRD patterns for $Ce_yZr_{1-y}O_2$ samples that had been calcined at 1323 K for 4 h: (a) $y = 0.81$, (b) $y = 0.59$, (c) $y = 0.33$, and (d) $y = 0.14$. The inset shows an expanded view of region associated with the (2 2 0) peak for cubic samples.

agreed very well with the known compositions. Although some of the materials may not be single phase, we calculated average crystallite sizes using the width of the (2 2 0) peak and the Debye–Scherrer equation.

Fig. 2 shows the diffraction patterns for selected samples after calcination at 1323 K for 4 h. The high-ceria sample, $Ce_{0.81}Zr_{0.19}O_2$, remained cubic, with the only change being an increase in the crystallite size, as indicated by the sharpening of the XRD lines. The two samples with intermediate compositions, $Ce_{0.59}Zr_{0.41}O_2$ and $Ce_{0.33}Zr_{0.67}O_2$, were unstable and separated into two phases, as expected [35,38]. The compositions of the two phases in each sample could be estimated from the lattice parameters, and the fraction of material in each phase could then be calculated using the lever rule. This calculation indicated that $Ce_{0.59}Zr_{0.41}O_2$ sample existed as a mixture of $Ce_{0.78}Zr_{0.22}O_2$ (71 wt.%) and $Ce_{0.13}Zr_{0.87}O_2$ (29 wt.%) after calcination at 1323 K, while $Ce_{0.33}Zr_{0.67}O_2$ existed as a mixture of $Ce_{0.79}Zr_{0.21}O_2$ (22 wt.%) and $Ce_{0.20}Zr_{0.80}O_2$ (78 wt.%). Finally, the low-ceria sample, $Ce_{0.14}Zr_{0.86}O_2$, remained single phase but exhibited a pattern indicative of the tetragonal zirconia structure.

2.2. Oxygen isotherms

Most of the oxygen isotherms were measured in a flow reactor, using techniques that have been described elsewhere [35]. Between 0.5 and 1.0 g of sample were placed in a quartz tube and then either oxidized in flowing air or reduced in dry flowing H_2 at the temperature of interest for 1 h. Each sample was then exposed to a flowing H_2–H_2O mixture (30 ml/min) at the same temperature for 3 h. The water vapor was introduced into the gas stream by passing H_2 through a temperature-controlled, water bubbler and the H_2O partial pressure was evaluated from the equilibrium vapor pressure. The H_2O:($H_2 + H_2O$) ratios of H_2–H_2O mixtures along with corresponding $P(O_2)$ are listed in Table 2. After equilibration of the sample in the H_2–H_2O mixture, the reactor was purged with dry He for 0.5 h. Finally, the oxidation state of the sample was determined by measuring the amount of oxygen required

Table 2
A list of the accessible oxygen partial pressure for the flow-titration and coulometric titration experiments

Temperature (K)	Flow system experiment		Coulometric titration, log($P(O_2)$) (atm)
	log($P(O_2)$) (atm)	H_2O/($H_2 + H_2O$) (%)[a]	
873	−28.9	0.3[b]	−21 to −14
	−28.3	0.6	
	−27.9	1	
	−26.9	3	
	−25.8	10	
	−24.6	30	
	−23.9	50	
973	−25.9	0.3	−17 to −2
	−25.3	0.6	
	−24.8	1	
	−23.9	3	
	−22.7	10	
	−21.6	30	
	−20.8	50	
1073	−23.4	0.3	−15 to −2
	−22.8	0.6	
	−22.3	1	
	−21.4	3	
	−20.3	10	
	−19.1	30	
	−18.4	50	

[a] H_2O is provided by flowing pure H_2 through a water bubbler.
[b] Additional amounts of pure H_2 were added to dilute the H_2O content at this composition.

for complete re-oxidation at the same temperature. This was accomplished by flowing air (21% O_2 and 79% N_2) over the sample at a rate of 4.3 ml/min and measuring the composition of the effluent gas from the reactor using a quadrupole mass spectrometer. The N_2 signal from the air was used as an internal standard for determining the amount of O_2 consumed; because the O_2 and N_2 signals showed clear break-through times, accurate measurements of O_2 consumption could be obtained. After re-oxidation of the sample, the reactor was again purged with dry He for 0.5 h.

It was possible to show that equilibrium was achieved by the fact that the extent of reduction was independent of whether we started with an oxidized or reduced sample. However, equilibrium was reached more quickly starting with samples that had been reduced in dry H_2 prior to exposing them to H_2–H_2O mixtures. We also observed that equilibrium was achieved more quickly when the samples were doped with 1 wt.% Pd; however, in the present study, Pd doping was used only on the $Ce_{0.14}Zr_{0.86}O_2$ sample. The Pd was added using an aqueous solution of $(NH_3)_4Pd(NO_3)_2$ (99.9%, Alfa Aesar), after which the sample was calcined at 723 K in air for an additional 5 h.

Because the range of $P(O_2)$ that could be accessed in the flow reactor was limited to lower values by our ability to control the $P(H_2O)/P(H_2)$ ratio (i.e. 10^{-26} atm $< P(O_2) < 10^{-21}$ atm at 973 K), some isotherms were measured using Coulometric Titration [31,34,36,39–48]. In Coulometric Titration, the sample is placed in a sealed container with an ion-conducting

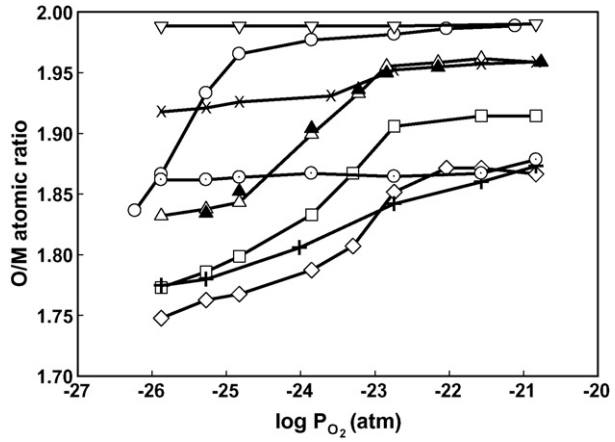

Fig. 3. Oxygen to total metal-ion (Ce + Zr) ratios for the $Ce_yZr_{1-y}O_{2-x}$ samples, following sample calcination at 973 K, as a function of $P(O_2)$. The y values in the samples are as follows: (○) $y = 1$, (△) $y = 0.92$, (□) $y = 81$, (◇) $y = 0.59$, (+) $y = 0.5$, (⊙) $y = 0.25$, (×) $y = 0.14$, and (▽) $y = 1.0$. The closed symbols for $y = 0.08$ (▲) were obtained from the sample after calcination at 1323 K for 4 h.

membrane (usually yttria-doped zirconia) separating the inside from the outside of the container. Oxygen is added or removed from the container by placing a potential across the membrane; so long as the membrane is strictly an ion conductor, the amount of oxygen transferred can be calculated from the amount of charge that has been transferred, as determined using a potentiometer. At open circuit, the membrane and its electrodes are used as an oxygen sensor, with the potential across the membrane related to the $P(O_2)$ in the container through the Nernst Equation. Unfortunately, because our system used Pt electrodes, we were unable to obtain data for very low $P(O_2)$ (i.e. the minimum $P(O_2)$ at 973 K was 10^{-19} atm) because of the tendency of Pt to react with ZrO_2 to form $PtZr_3$ [40]. This led to a small gap in the isotherms between the low-$P(O_2)$ region measured using the flow system and the high-$P(O_2)$ region measured using Coulometric titration.

3. Results and discussion

3.1. Samples calcined to 973 K

To characterize the single-phase, ceria–zirconia solid solutions, we first examined the properties of materials that had been calcined only at 973 K. Fig. 3 shows isotherms at 973 K for ceria, zirconia, and a series of ceria–zirconia solid solutions having a wide range of compositions. Pure ZrO_2 showed minimal reduction in all cases, as expected. The isotherm for pure ceria also agreed well with published data [27]. It is worth noting again that ceria is almost completely oxidized (O:Ce = 1.98) at 973 K and a $P(O_2)$ of 10^{-23} atm, conditions that correspond to a gas mixture consisting of 8% H_2O and 92% H_2. The data in Fig. 3 show that the properties of the solid solutions cannot be described as physical mixtures of ceria and zirconia. Each of the solid solutions underwent reduction at much higher values of $P(O_2)$ than is observed for pure CeO_2 or ZrO_2. For example, the $Ce_{0.92}Zr_{0.08}O_2$ sample is significantly more reduced than CeO_2 at all $P(O_2)$ between 10^{-21} and 10^{-26} atm. Furthermore, calcining the $Ce_{0.92}Zr_{0.08}O_2$ sample to 1323 K for 4 h had no effect on the oxygen isotherm, even though this treatment significantly increased the crystallite size, as shown in Table 1.

A distinctive feature in the isotherms of all of the ceria–zirconia solutions is that there is a plateau region at the highest accessible $P(O_2)$, with the O:M ratio remaining constant for a significant range of $P(O_2)$ values. With the $Ce_{0.92}Zr_{0.08}O_2$ and $Ce_{0.81}Zr_{0.19}O_2$ samples, these plateaus occur at O:M ratios of approximately 1.96 and 1.90; it is probably significant that the compositions at these plateaus can be considered a combination of CeO_2 and the pyrochlore structure [36], $Ce_2Zr_2O_7$ (e.g. $Ce_{0.81}Zr_{0.19}O_{1.905}$ can be written as $0.62\ CeO_2 + 0.095\ Ce_2Zr_2O_7$). XRD did not show any special phases associated with the ''plateau'' oxidation state [35], implying that there is no bulk pyrochlore present. However we suggest that pyrochlore clusters are forming on the atomic scale, as discussed elsewhere [36].

Solid solutions with roughly equal amounts of Ce and Zr ($Ce_{0.59}Zr_{0.41}O_2$ and $Ce_{0.50}Zr_{0.50}O_2$) were the most reducible. From a scientific point of view, it is also interesting to consider the two high-zirconia samples, $Ce_{0.25}Zr_{0.75}O_2$ and $Ce_{0.14}Zr_{0.86}O_2$. The isotherm data for $Ce_{0.25}Zr_{0.75}O_2$ indicated the O:M ratio was ~1.87 at all $P(O_2)$ that were accessible using flow titration with H_2–H_2O mixtures. The O:M ratio for complete reduction of Ce^{4+} to Ce^{3+} would be 1.875. For $Ce_{0.14}Zr_{0.86}O_2$, the O:M ratio at the lowest $P(O_2)$ is also close to what would be expected for complete reduction of Ce^{4+}, 1.93. Since pure zirconia shows a slight reduction (O:M = 1.98), we suggest that the slight over-reduction of $Ce_{0.14}Zr_{0.86}O_2$ may be associated with reduction of surface zirconia. However, unlike the $Ce_{0.25}Zr_{0.75}O_2$ sample, we observed that the $Ce_{0.14}Zr_{0.86}O_2$ sample progressively oxidized as the $P(O_2)$ increased. Because removal of an O^{2-} ion requires reduction of two Ce^{4+} ions, it is likely that spatially isolated Ce^{4+} ions in $Ce_{0.14}Zr_{0.86}O_2$ are more stable and are therefore more difficult to reduce. The metal ions in the fluorite structure have 12 nearest-neighbor ions, implying that essentially all of the Ce^{4+} ions in $Ce_{0.25}Zr_{0.75}O_2$ can couple with other Ce^{4+} ions, while the same will not be true for $Ce_{0.14}Zr_{0.86}O_2$.

Fig. 4a–d displays the oxygen isotherms at 873, 973, and 1073 K for the $Ce_{0.81}Zr_{0.19}O_2$, $Ce_{0.5}Zr_{0.5}O_2$, $Ce_{0.25}Zr_{0.75}O_2$, and $Ce_{0.14}Zr_{0.86}O_2$ samples, after the samples had been calcined at only 973 K to avoid formation of two phases. The shapes of the isotherms were unaffected by temperature but the shift in those isotherms allowed determination of the oxidation enthalpies using Eq. (2). Fig. 5 displays the oxidation enthalpies determined from the data in Fig. 4; Fig. 6 displays the oxidation entropies, calculated from the differences between ΔG and ΔH. The oxidation enthalpies and entropies are also summarized in Table 3. The data for the $Ce_{0.81}Zr_{0.19}O_2$ and $Ce_{0.25}Zr_{0.75}O_2$ have been presented in detail elsewhere [36] and will be discussed here only briefly.

For the $Ce_{0.81}Zr_{0.19}O_2$ sample, the equilibrium data in Fig. 4a show oxidation occurs in two $P(O_2)$ regions at all three temperatures. In the lower $P(O_2)$ region, $Ce_{0.81}Zr_{0.19}O_{1.8}$

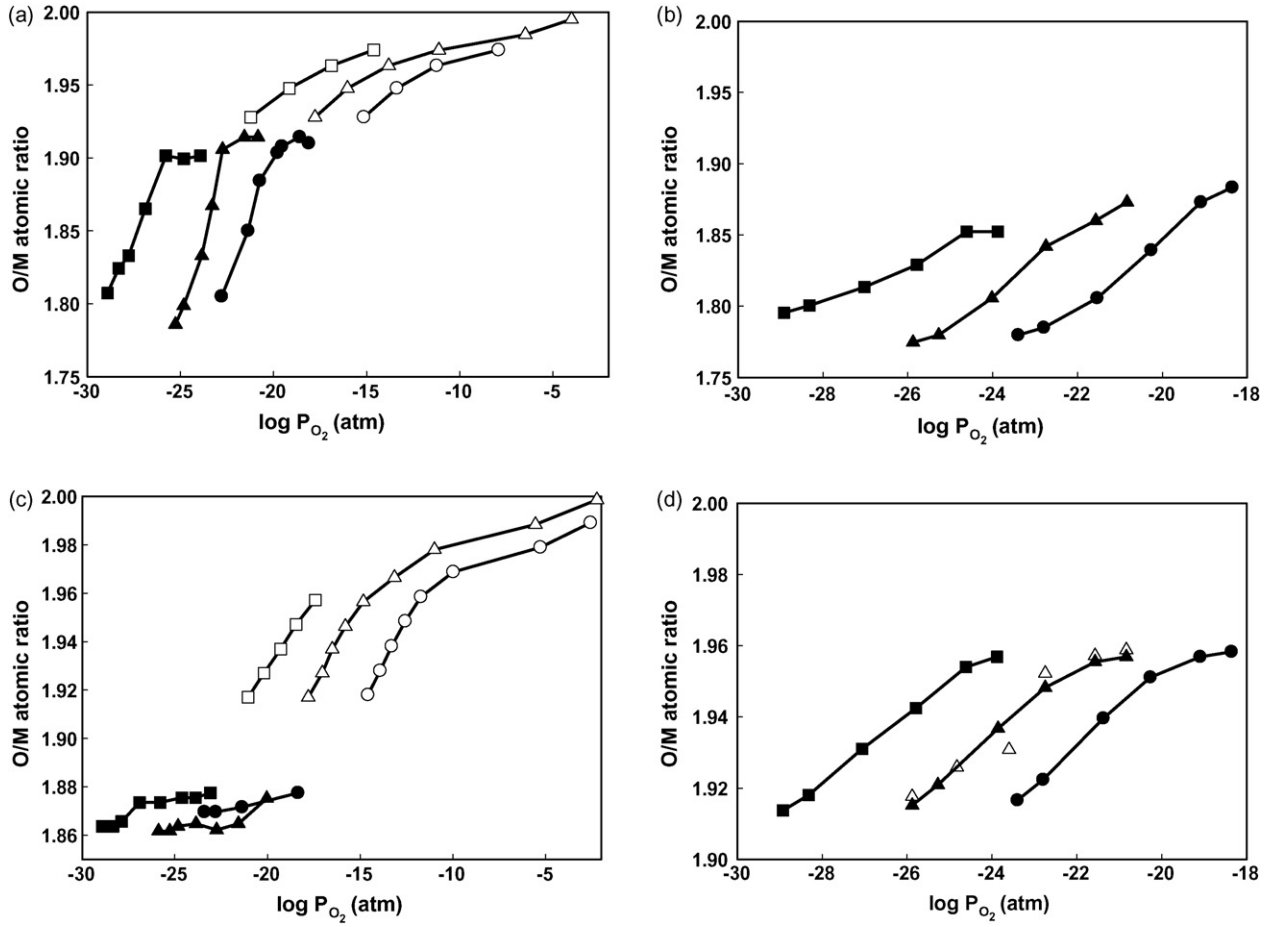

Fig. 4. (a) O:M (Ce + Zr) ratios for $Ce_{0.81}Zr_{0.19}O_{2-x}$ as a function of $P(O_2)$ and temperature ((■) 873 K; (▲) 973 K; (●) 1073 K). Open symbols denote data from Coulometric titration and closed symbols denote data from flow-titration experiments. (b) O:M (Ce + Zr) ratios for $Ce_{0.5}Zr_{0.5}O_2$ as a function of $P(O_2)$ and temperature ((■) 873 K; (▲) 973 K; (●) 1073 K). (c) O:M (Ce + Zr) ratios for $Ce_{0.25}Zr_{0.75}O_{2-x}$ as a function of $P(O_2)$ and temperature ((■) 873 K; (▲) 973 K; (●) 1073 K). Open symbols denote data from Coulometric titration and closed symbols denote data from flow-titration experiments. (d) O:M (Ce + Zr) ratios for 1 wt.% Pd on $Ce_{0.14}Zr_{0.86}O_2$ as a function of $P(O_2)$ and temperature ((■) 873 K; (▲) 973 K; (●) 1073 K). The data shown with open symbols (△) were obtained on the $Ce_{0.14}Zr_{0.86}O_2$ with no Pd at 973 K, while the other data were obtained on a sample containing 1 wt.% Pd.

becomes oxidized to a stoichiometry of $Ce_{0.81}Zr_{0.19}O_{1.90}$, at which point the oxygen stoichiometry remains at a constant value over a considerable range of $P(O_2)$. The oxidation of $Ce_{0.81}Zr_{0.19}O_{1.90}$ to $Ce_{0.81}Zr_{0.19}O_2$ occurs only at higher $P(O_2)$. Surprisingly, the oxidation enthalpies calculated from this data fall between −500 and −550 kJ/mol O_2 in both regions, and there are no obvious changes in the oxidation enthalpies with the extent of reduction. The values for $-\Delta H$ are lower than that

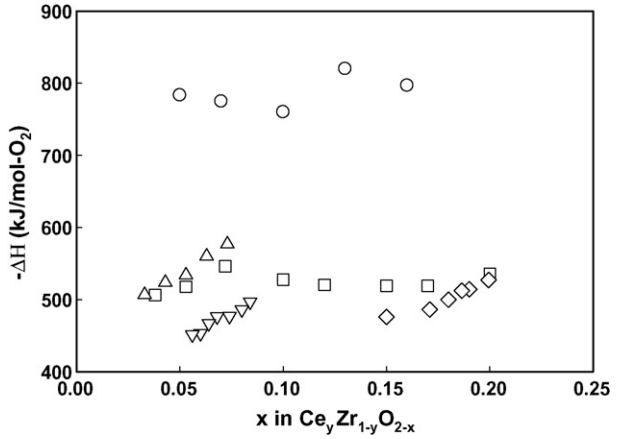

Fig. 5. ΔH of oxidation at 973 K for $Ce_yZr_{1-y}O_{2-x}$ as a function of extent of reduction: (○) $y = 1$, (□) $y = 0.81$, (◇) $y = 0.5$, (△) $y = 0.25$, and (▽) $y = 0.14$.

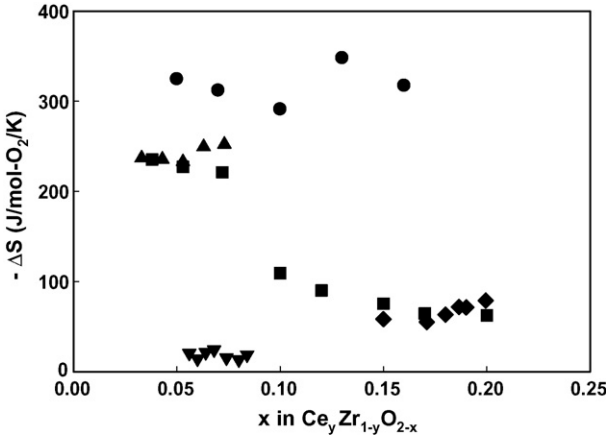

Fig. 6. ΔS of oxidation at 973 K for $Ce_yZr_{1-y}O_{2-x}$ as a function of extent of reduction: (●) $y = 1$, (■) $y = 0.81$ (◆) $y = 0.5$, (▲) $y = 0.25$, and (▼) $y = 0.14$.

Table 3
The measured oxidation enthalpies and entropies for each of the samples examined in this study

Sample	x in $Ce_yZr_{1-y}O_{2-x}$	$-\Delta H$ (kJ/mol O_2)	$-\Delta S$ (J/mol O_2/K)
CeO_{2-x}	0.05	783	325
	0.07	775	312
	0.10	760	291
	0.13	820	348
	0.16	797	317
$Ce_{0.81}Zr_{0.19}O_{2-x}$	0.20	536	62
	0.17	519	65
	0.15	519	75
	0.12	520	90
	0.10	528	109
	0.07	546	221
	0.05	518	227
	0.04	506	235
$Ce_{0.5}Zr_{0.5}O_{2-x}$	0.20	527	79
	0.19	514	71
	0.19	512	72
	0.18	500	63
	0.17	486	55
	0.15	476	58
$Ce_{0.25}Zr_{0.75}O_{2-x}$	0.07	577	252
	0.06	560	249
	0.05	534	233
	0.04	524	236
	0.03	507	237
$Ce_{0.14}Zr_{0.86}O_{2-x}$	0.08	497	19
	0.08	486	13
	0.07	477	16
	0.07	476	24
	0.06	467	21
	0.06	453	14
	0.06	451	21

obtained for pure CeO_2 (-760 kJ/mol O_2 [49]) by approximately 240 kJ/mol, which partially explains the comparative ease the solid solutions undergo reduction. Of additional interest, $-\Delta H$ is essentially independent of oxygen stoichiometry. Even though the oxygen isotherms exhibit distinct ranges of $P(O_2)$ for reduction of $Ce_{0.81}Zr_{0.19}O_2$ to $Ce_{0.81}Zr_{0.19}O_{1.9}$ and reduction of $Ce_{0.81}Zr_{0.19}O_{1.9}$ to $Ce_{0.81}Zr_{0.19}O_{1.8}$, the differential enthalpy changes are the same in both ranges. It is also interesting to consider that the enthalpies determined here are very close to the enthalpies of oxidation for pyrochlore, $Ce_2Zr_2O_7$. Using equilibrium data from the literature for the oxidation of the pyrochlore [34], we have calculated enthalpies of oxidation for this compound to be between -520 and -540 kJ/mol O_2.

Isotherms at the three temperatures for $Ce_{0.5}Zr_{0.5}O_2$ are shown in Fig. 4b. Since measurements were only performed in the flow reactor, the range of O:M ratios that were sampled was more limited, but the oxidation enthalpies were again determined to be between -480 and -530 kJ/mol. At all three temperatures, a significant fraction of the Ce metal ions remained as Ce^{4+} at the lowest $P(O_2)$ accessible in this study. For the $Ce_{0.25}Zr_{0.75}O_2$ sample, Fig. 4c, the O:M stoichiometry remained between 1.87 and 1.88 for the accessible range of $P(O_2)$ in the flow-titration reactor, making it necessary to use Coulometric titration to gain any information about oxidation enthalpies at higher $P(O_2)$. As with $Ce_{0.81}Zr_{0.19}O_2$, the oxidation enthalpies fell between -500 and -550 kJ/mol O_2. Finally, the isotherms for $Ce_{0.14}Zr_{0.86}O_2$ are shown in Fig. 4d. The oxidation enthalpies that we calculate from this data appear to be slightly lower in magnitude, between -450 and -500 kJ/mol O_2, but this difference is certainly small compared to the very large differences in oxidation enthalpies between the ceria–zirconia samples and that of pure CeO_2.

Since the oxidation enthalpies of the solid solutions are almost the same in each case, the important features differentiating the adsorption isotherms of the various ceria–zirconia solid solutions result primarily from entropy effects, as shown in Fig. 6. In agreement with the literature [27–29,33], the magnitudes of the partial molar entropies for oxidation of pure CeO_2, calculated from our data, are relatively large, between -300 and -350 J/mol K. The high entropy change for CeO_2 is due to the large number of equivalent sites from which oxygen can be removed from the fluorite lattice. For oxidation of $Ce_{0.25}Zr_{0.75}O_{1.88}$ and oxidation of $Ce_{0.81}Zr_{0.19}O_{1.9}$ to $Ce_{0.81}Zr_{0.19}O_2$, the magnitudes of the entropy changes are almost as large as for CeO_2, approximately -250 J/mol K, which suggests oxygen can again be removed from a large number of possible sites. However, for oxidation of $Ce_{0.81}Zr_{0.19}O_{1.8}$ to $Ce_{0.81}Zr_{0.19}O_{1.9}$, the magnitude of the partial molar oxidation entropy is much lower, between -50 and -100 J/mol K, which suggests a small number of sites are involved. The entropy change for oxidation of $Ce_{0.14}Zr_{0.86}O_{1.93}$ is nearly zero (circa -20 J/mol K), which implies the system is highly ordered.

Previously, we suggested that the oxidation enthalpies and entropies for the solid solutions could be explained by viewing oxidation and reduction as a strictly local phenomenon [36]. Each metal cation in the fluorite lattice has 12 nearest neighbors and each oxygen anion is in contact with four metal cations. If one assumes that the energetics of oxidation are strictly local, that the energy to remove an oxygen ion depends only on the four metal cations that are in direct contact with that oxygen ion, then the energy associated with adding or removing an oxygen atom will not depend on the bulk composition. Furthermore, adding an oxygen ion to a site surrounded by two Ce^{3+} cations and two Zr^{4+} cations should be energetically similar to adding an oxygen atom to the pyrochlore structure. Indeed, the oxidation enthalpies for each of the ceria–zirconia solutions are identical to what has been reported for oxidation of the pyrochlore, $Ce_2Zr_2O_7$.

More importantly, this model can explain some of the entropic effects that affect the isotherm. For example, for oxidation of $Ce_{0.81}Zr_{0.19}O_{1.9}$ to $Ce_{0.81}Zr_{0.19}O_2$, the entropy change is large. This is because each Zr^{4+} cation in the structure can be thought of as being paired with one or more other Zr^{4+} cations and each pair of Zr^{4+} cations can interact with a large number of Ce^{n+} cations in its vicinity. The large number of ways an oxygen atom can be removed from a site that is surrounded by two Zr^{4+} and two Ce^{n+} results in a high entropy

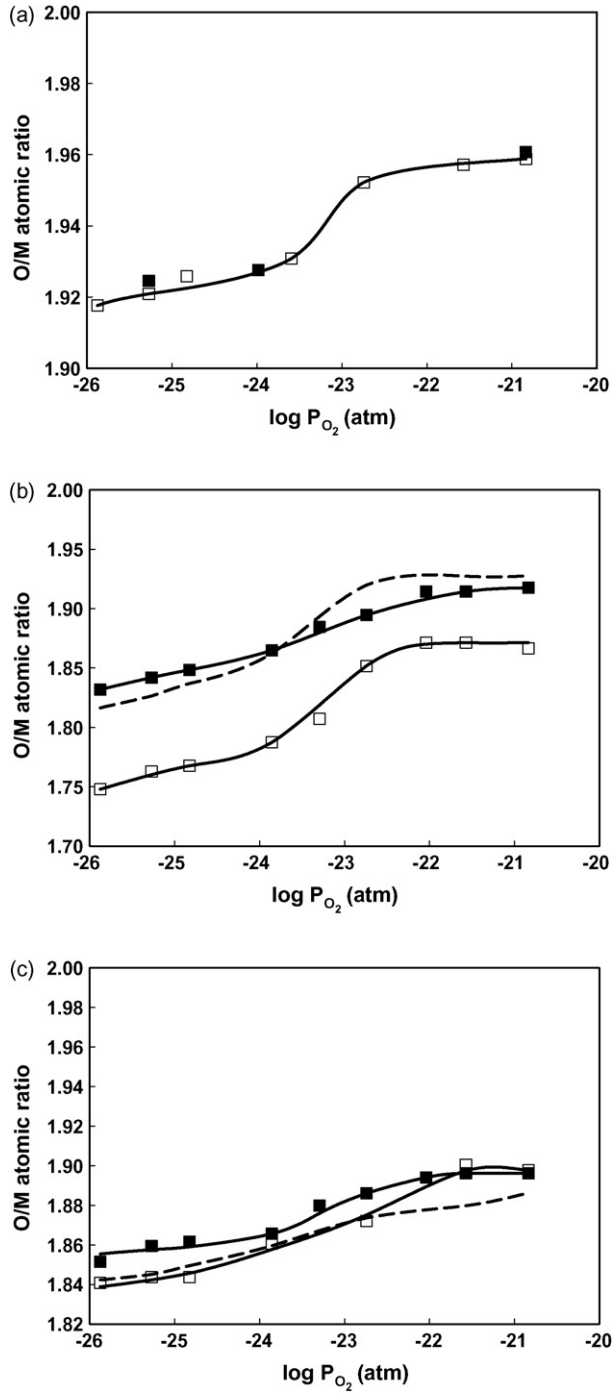

Fig. 7. (a) O:M ratios as a function of $P(O_2)$ for $Ce_{0.14}Zr_{0.86}O_2$ sample after calcination at 973 K (□) and 1323 K for 4 h (■). (b) O:M ratios as a function of $P(O_2)$ for the $Ce_{0.59}Zr_{0.41}O_2$ sample after calcination at 973 K (□) and 1323 K for 4 h (■). The simulated result (- - -) was calculated by assuming the sample calcined to 1323 K could be modeled as a physical mixture of $Ce_{0.81}Zr_{0.19}O_2$ and $Ce_{0.13}Zr_{0.87}O_2$. (c) O:M ratios as a function of $P(O_2)$ for the $Ce_{0.33}Zr_{0.67}O_2$ sample after calcination at 973 K (□) and 1323 K for 4 h (■). The simulated result (- - -) was calculated by assuming the sample calcined to 1323 K could be modeled as a physical mixture of $Ce_{0.81}Zr_{0.19}O_2$ and $Ce_{0.25}Zr_{0.75}O_2$.

change. Once each pair of Zr^{4+} cations is part of a $(Zr^{4+}–Ce^{3+})_2$ cluster, a point reached at the plateau stoichiometry (e.g. $Ce_{0.81}Zr_{0.19}O_{1.9}$), the number of ways in which these two Zr^{4+} cations can be used in forming a second cluster is limited—at least if there is a repulsion between oxygen vacancies. Hence, the number of oxygen atoms available for removal decreases at a stoichiometry corresponding to all of the Zr^{4+} being part of a reduced pyrochlore cluster. Similarly for $Ce_{0.14}Zr_{0.86}O_2$, the entropies are near zero because only specific O^{2-} anions associated with two Ce^{4+} ions can be easily removed from the lattice.

3.2. Samples calcined to 1323 K

To determine the effect of high-temperature calcination and phase separation of the solid solutions, we examined selected materials that had been heated in air to 1323 K for 4 h. As discussed earlier, this treatment had no effect on the structure of the $Ce_{0.92}Zr_{0.08}O_2$ sample as measured by XRD and no effect on the equilibrium isotherm of this sample, as shown by the data in Fig. 3. While calcination of the $Ce_{0.14}Zr_{0.86}O_2$ sample up to 1323 K caused changes in the XRD, i.e. formation of a clearly tetragonal structure, Fig. 7a shows that this pretreatment did not lead to any changes in the equilibrium isotherm measured at 973 K.

It is more interesting to consider the effect of high-temperature calcination on solid solutions with intermediate compositions, $Ce_{0.59}Zr_{0.41}O_2$ and $Ce_{0.33}Zr_{0.67}O_2$, since XRD showed these compositions to be unstable. Fig. 7b, which provides a comparison of isotherms on $Ce_{0.59}Zr_{0.41}O_2$ following calcination to either 973 or 1323 K, shows that the isotherm is shifted to higher O:M ratios following the 1323 K treatment. The effect of calcination is simply the result of changes in the phases present in the sample. Based on the XRD results discussed earlier, we estimated that the $Ce_{0.59}Zr_{0.41}O_2$ decomposed into $Ce_{0.78}Zr_{0.22}O_2$ (71 wt.%) and $Ce_{0.13}Zr_{0.87}O_2$ (29 wt.%) phases. Assuming that $Ce_{0.78}Zr_{0.22}O_2$ would have a nearly identical isotherm to that of $Ce_{0.81}Zr_{0.19}O_2$ and $Ce_{0.13}Zr_{0.87}O_2$ as that of $Ce_{0.14}Zr_{0.86}O_2$, we calculated that the isotherm of the 1323 K sample would be that of the dashed line in Fig. 7b. It is clear that the calculated result agrees very well with the measured isotherm. Similarly, $Ce_{0.33}Zr_{0.67}O_2$ decomposed into $Ce_{0.79}Zr_{0.21}O_2$ (22 wt.%) and $Ce_{0.20}Zr_{0.80}O_2$ (78 wt.%) phases following calcination to 1323 K. Fig. 7c shows that the O:M ratios for the $Ce_{0.33}Zr_{0.67}O_2$ after calcination to 1323 K were again slightly higher at each $P(O_2)$. The simulated isotherm, the dashed line calculated from isotherms of $Ce_{0.81}Zr_{0.19}O_2$ and $Ce_{0.25}Zr_{0.75}O_2$, is slightly lower than the measured isotherms, especially at high $P(O_2)$. This could be due to difference in the isotherms between $Ce_{0.20}Zr_{0.80}O_2$ and $Ce_{0.25}Zr_{0.75}O_2$. Despite the difference, the simulated isotherm curve agreed well with the experimentally measured result.

The obvious conclusion from this data is that the calcination temperature of the solid solutions affects the thermodynamic redox properties primarily through the changes in the phases that are formed. This is very significant in that high-temperature calcination also changes the crystallite size and sample surface areas. One should certainly expect that changes in the crystallite size would affect the kinetics of reduction and oxidation.

4. Conclusions

The following observations can be drawn from this study:

(1) The thermodynamic redox properties of ceria–zirconia solid solutions depend primarily on the composition of the oxides, rather that the oxide surface areas or crystallite sizes. When solid solutions were calcined to temperatures sufficient to cause phase separation, the thermodynamic properties were the same as would be expected for a physical mixture of the two phases.
(2) The oxidation enthalpies for all the ceria–zirconia solid solutions that were studied were independent of the extent of cerium reduction and between −500 and −550 kJ/mol O_2, a value similar to that found for oxidation of the pyrochlore, $Ce_2Zr_2O_7$. The oxidation entropies depended on sample composition and the extent of ceria reduction.
(3) The thermodynamic properties for oxidation of ceria–zirconia solid solutions can be understood from a simple model that considers the energetics of removing an oxygen to be related only to the four nearest-neighbor metal cations. The oxidation entropies are affected by the number of possible oxygens that can be removed from a particular structure.

Acknowledgements

This work was supported by the Department of Energy, Office of Basic Energy Sciences, Chemical Sciences, Geosciences and Biosciences Division, Grant DE-FG02-85ER13350.

References

[1] R.W. Mccabe, J.M. Kisenyi, Chem. Ind. (1995) 605.
[2] M. Shelef, G.W. Graham, R.W. McCabe, in: A. Trovarelli (Ed.), Catalysis by Ceria and Related Materials, Imperial College Press, London, 2002.
[3] J. Kaspar, P. Fornasiero, N. Hickey, Catal. Today 77 (2003) 419.
[4] M. Sugiura, M. Ozawa, A. Suda, T. Suzuki, T. Kanazawa, Bull. Chem. Soc. Jpn. 78 (2005) 752.
[5] H. Shinjoh, J. Alloys Compd. 408–412 (2006) 1061.
[6] T. Masui, T. Ozaki, K.-I. Machida, G.-Y. Adachi, J. Alloys Compd. 303–304 (2000) 49.
[7] M. Ozawa, M. Kimura, A. Isogai, J. Alloys Compd. 193 (1993) 73.
[8] T. Bunluesin, R.J. Gorte, G.W. Graham, Appl. Catal. B: Environ. 15 (1998) 107.
[9] S.Y. Choung, M. Ferrandon, T. Krause, Catal. Today 99 (2005) 257.
[10] Q. Fu, H. Saltsburg, M. Flytzani-Stephanopoulos, Science 301 (2003) 935.
[11] A.F. Ghenciu, Curr. Opin. Solid State Mater. Sci. 6 (2002) 389.
[12] S. Hilaire, X. Wang, T. Luo, R.J. Gorte, J. Wagner, Appl. Catal. A: Gen. 215 (2001) 271.
[13] G. Jacobs, P.A. Patterson, U.M. Graham, D.E. Sparks, B.H. Davis, Appl. Catal. A: Gen. 269 (2004) 63.
[14] X.S. Liu, W. Ruettinger, X.M. Xu, R. Farrauto, Appl. Catal. B: Environ. 56 (2005) 69.
[15] S.L. Swartz, M.M. Seabaugh, C.T. Holt, W.J. Dawson, Fuel Cell Bull. 4 (2001) 7.
[16] R. Craciun, B. Shereck, R.J. Gorte, Catal. Lett. 51 (1998) 149.
[17] R. Farrauto, S. Hwang, L. Shore, W. Ruettinger, J. Lampert, T. Giroux, Y. Liu, O. Ilinich, Annu. Rev. Mater. Res. 33 (2003) 1.
[18] R.M. Heck, R.J. Farrauto, Appl. Catal. A: Gen. 221 (2001) 443.
[19] A. Bueno-Lopez, K. Krishna, M. Makkee, J. Moulijn, Catal. Lett. 99 (2005) 203.
[20] A. Bueno-Lopez, K. Krishna, M. Makkee, J.A. Moulijn, J. Catal. 230 (2005) 237.
[21] C. de Leitenburg, A. Trovarelli, J. Llorca, F. Cavani, G. Bini, Appl. Catal. A: Gen. 139 (1996) 161.
[22] T. Montini, M.A. Banares, N. Hickey, R. Di Monte, P. Fornasiero, J. Kaspar, M. Graziani, Phys. Chem. Chem. Phys. 6 (2004) 1.
[23] G. Dutta, U.V. Waghmare, T. Baidya, M.S. Hegde, K.R. Priolkar, P.R. Sarode, Catal. Lett. 108 (2006) 165.
[24] M.P. Yeste, J.C. Harnandez, S. Bernal, G. Blanco, J.J. Calvino, J.A. Perez-Omil, J.M. Pintado, Chem. Mater. 18 (2006) 2750.
[25] P. Fornasiero, R. Dimonte, G.R. Rao, J. Kaspar, S. Meriani, A. Trovarelli, M. Graziani, J. Catal. 151 (1995) 168.
[26] G. Brauer, K.A. Gingerich, U. Holtschmidt, J. Inorg. Nucl. Chem. 16 (1960) 77.
[27] D.J.M. Bevan, J. Kordis, J. Inorg. Nucl. Chem. 26 (1964) 1509.
[28] R.J. Panlener, R.N. Blumenthal, J.E. Garnier, J. Phys. Chem. Solids 36 (1975) 1213.
[29] O.T. Sorensen, J. Solid State Chem. 18 (1976) 217.
[30] J. Campserveux, P. Gerdanian, J. Solid State Chem. 23 (1978) 73.
[31] I. Riess, H. Janczikowski, J. Nolting, J. Appl. Phys. 61 (1987) 4931.
[32] M.A. Panhans, R.N. Blumenthal, Solid State Ionics 60 (1993) 279.
[33] M. Mogensen, N.M. Sammes, G.A. Tompsett, Solid State Ionics 129 (2000) 63.
[34] H. Otobe, A. Nakamura, T. Yamashita, K. Minato, J. Phys. Chem. Solids 66 (2005) 329.
[35] T. Kim, J.M. Vohs, R.J. Gorte, Ind. Eng. Chem. Res. 45 (2006) 5561.
[36] P.R. Shah, T. Kim, G. Zhou, P. Fornasiero, R.J. Gorte, Chem. Mater. 18 (2006) 5363.
[37] J. Kaspar, P. Fornasiero, G. Baiducci, R. Di Monte, N. Hickey, V. Sergo, Inorg. Chim. Acta 349 (2003) 217.
[38] G. Colon, M. Pijolat, F. Valdivieso, H. Vidal, J. Kaspar, E. Finocchio, M. Daturi, C. Binet, J.C. Lavalley, R.T. Baker, S. Bernal, J. Chem. Soc.-Faraday Trans. 94 (1998) 3717.
[39] R.A. Giddings, R.S. Gordon, J. Electrochem. Soc. 121 (1974) 793.
[40] J. Werner, R. Schmidfetzer, Thermochim. Acta 129 (1988) 127.
[41] D. Schneider, M. Godickemeier, L.J. Gauckler, J. Electroceram. 1 (1997) 165.
[42] Y.D. Tretyakov, A.F. Maiorova, Y.M. Berezovskaya, Electrical Properties of Oxide Materials, 1997, p. 283.
[43] S. Otsuka-Yao-Matsuo, N. Izu, T. Omata, K. Ikeda, J. Electrochem. Soc. 145 (1998) 1406.
[44] J.C.C. Abrantes, D. Perez-Coll, P. Nunez, J.R. Frade, Electrochim. Acta 48 (2003) 2761.
[45] V.N. Tikhonovich, O.M. Zharkovskaya, E.N. Naumovich, I.A. Bashmakov, V.V. Kharton, A.A. Vecher, Solid State Ionics 160 (2003) 259.
[46] S. Diethelm, J. Van herle, Solid State Ionics 174 (2004) 127.
[47] E. Bakken, T. Norby, S. Stolen, Solid State Ionics 176 (2005) 217.
[48] C.Y. Park, A.J. Jacobson, J. Electrochem. Soc. 152 (2005) J65.
[49] D.R. Lide, CRC Handbook of Chemistry and Physics, CRC Press, Boca Raton, FL, 2005.